Accepted Manuscript

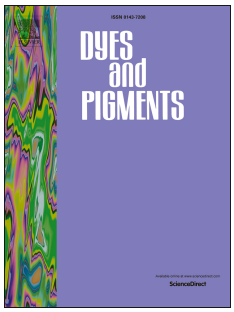

Rational construction of probes rendering ratiometric response to the cancer-specific enzyme NQO1

Qiang Fei, Li Zhou, Feiyi Wang, Ben Shi, Chunbao Li, Rui Wang, Chunchang Zhao

PII: S0143-7208(16)30721-5

DOI: 10.1016/j.dyepig.2016.09.031

Reference: DYPI 5483

To appear in: *Dyes and Pigments*

Received Date: 27 June 2016

Revised Date: 3 September 2016

Accepted Date: 12 September 2016

Please cite this article as: Fei Q, Zhou L, Wang F, Shi B, Li C, Wang R, Zhao C, Rational construction of probes rendering ratiometric response to the cancer-specific enzyme NQO1, *Dyes and Pigments* (2016), doi: 10.1016/j.dyepig.2016.09.031.

Graphical abstract

Rational Construction of Probes Rendering Ratiometric Response to the Cancer-Specific Enzyme NQO1

Qiang Fei, Li Zhou, Feiyi Wang, Ben Shi, Chunbao Li, Rui Wang, Chunchang Zhao

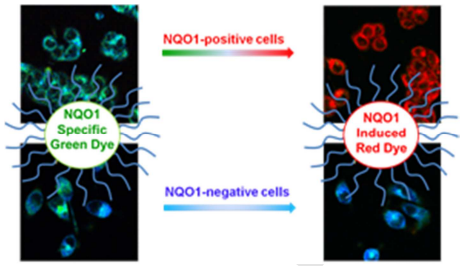

Rational Construction of Probes Rendering Ratiometric Response to the Cancer-Specific Enzyme NQO1

Qiang Fei,[a,b] Li Zhou,[c] Feiyi Wang,[b] Ben Shi,[b] Chunbao Li,[a,*] Rui Wang,[c] Chunchang Zhao[b,*]

a. *Department of Chemistry, School of Science, Tianjin University, Tianjin 300072 (China), E-Mail: lichunbao@tju.edu.cn*

b. *Key Laboratory for Advanced Materials and Institute of Fine Chemicals, East China University of Science & Technology, Shanghai 200237 (China), E-Mail: zhaocchang@ecust.edu.cn*

c. *Shanghai Key Laboratory of New Drug Design, School of Pharmacy, East China University of Science & Technology, Shanghai 200237 (China)*

Keywords: cancer biomarker, polymeric micelle, nanoprobe, ratiometric, cancer-specific NQO1

Abstract

Pursuit of fluorescent probes for identification of cancer biomarkers benefits reliable predictions of early cancer detection. Here, a strategy employing polymeric micelle assembly for encapsulation of a new enzyme (NQO1)-responsive small molecule was established for facile access to nanoprobes with favorable features in bioimaging, such as good aqueous solubility, enhanced photo-stability and biocompatibility. In the presence of the enzyme NQO1, these nanoprobes underwent ratiometric fluorescence changes from yellow-green fluorescence signals to red fluorescence signals. By exploiting this favorable ratiometric response to NQO1, we explored these nanoprobes for evaluation of enzyme activity in living cells, which showed distinct differentiation between NQO1-positive cancer cells and NQO1-negative cells.

1. Introduction

Growing evidence indicates that identification of cancer biomarkers can render great promise for highly reliable predictions of early cancer detection [1-2]. Thereby, there currently exists extensive interest in the pursuit of fluorescent probes for the detection of crucial species, such as enzymes, intending to target the bio-imaging of tumor cells [3-25]. Among many potential enzyme biomarkers, NAD(P)H:quinone oxidoreductase isozyme 1 (NQO1) is an endogenous enzyme that is overexpressed in a number of tumors, including colon, breast, liver and lung cancers, at levels of 2- to 50 fold greater than in surrounding normal tissue [26]. NQO1 can specifically catalyze a two-electron reduction of various quinones directly to the hydroquinone [27], inferring that profluorophores or prodrugs containing a quinone moiety that are activated by NQO1 should show dramatic tumor-specific activity. Indeed, it has been realized that the catalytic property of NQO1 makes this enzyme an ideal biomarker for cancer

diagnosis as well as a therapeutic target [28, 29].

Despite the great implication of NQO1 as a biomarker for early diagnosis, only a few fluorescent probes, to our knowledge, were reported for evaluation of this cancer-linked enzyme [30-33]. Furthermore, these reported probes fulfill fluorescence turn-on functions by specific NQO1-mediated removal of the quinone cage. However, such fluorescence turn-on mode is susceptible to experimental conditions. It is therefore highly desirable to develop more reliable and versatile probes with ratiometric response which can greatly eliminate experimental interferences through self-calibration effect [34-38]. Another bottleneck encountered with common organic probes lies in the fact that they always suffer from the limitation of low aqueous solubility, poor photo- and chemical stability, which are detrimental to the practical application in native biological media.

With all these considerations in mind, we report the polymeric micelle assembly for facile access to nanoprobes rendering a ratiometric response to cancer-specific NQO1, representing a design strategy that has been unexplored. To this end, we firstly designed a small molecule probe BOD-NQO1 by tethering an NQO1 trigger (a trimethyl-locked quinone propionic acid) to a 6-hydroxylphenol-BODIPY platform through a linker *p*-aminobenzyl alcohol (Scheme 1). Interestingly, reductant-mediated conversion of the trimethyl-locked quinone to hydroquinone triggered lactonization to liberate *p*-aminobenzyloxycarbonate, which then underwent self-immolation to deliver the red fluorescent 6-hydroxylphenol-BODIPY dye. Unfortunately, the poor solubility of BOD-NQO1 in aqueous solution (common issue encountered with organic probes) seriously retards its direct assay of NQO1 activity. To surpass this inconvenience, BOD-NQO1 was embedded into the hydrophobic interior of a polymeric micelle assembly based

on an amphiphilic copolymer mPEG-DSPE (1,2-dimyristoyl-sn-glycero-3-phosphorethanolamine-*N*-(methoxy(polyethylene glycol)-2000)) [39-41], and a nanoprobe (in short Nano-NQO1) was thus created (Scheme 1). This encapsulation endowed Nano-NQO1 excellent aqueous solubility, significantly enhanced chemical and photo-stability as well as biocompatibility. Satisfyingly, Nano-NQO1 displayed favorable ratiometric response to NQO1, which has been successfully exploited for discriminative imaging of NQO1-positive cells.

2. Experimental Section

2.1. Materials and instruments

All chemical reagents and solvents for synthesis were purchased from commercial suppliers and were used without further purification. ^{1}H NMR and ^{13}C NMR spectra were recorded on a Bruker AV-400 spectrometer with chemical shifts reported in ppm at room temperature. Mass spectra were measured on a HP 1100 LC-MS spectrometer.

UV-vis absorption spectra were recorded on a Varian Cary 100 spectrophotometer. Fluorescence spectra were measured with a Varian Cary Eclipse Fluorescence spectrophotometer.

2.2. Synthesis

Compound **1** was synthesized according to literature procedures [42]. HO-BODIPY was obtained according to previous work in our group [43].

*2.2.1. 4-(((tert-butyldimethylsilyl)oxy)methyl)aniline **2***

To a solution of 4-aminobenzyl alcohol (2.0 g, 16.24 mmol) in dry DMF (20 mL) were added tert-butyldimethylsilyl chloride (3.67 g, 24.35 mmol) and imidazole (2.21 g, 32.46 mmol), the resulting mixture was further stirred for 5 h at room temperature. The reaction mixture was then diluted with

saturated brine solution and extracted with CH_2Cl_2. The organic layer was separated and washed with brine solution for several times, then dried over anhydrous Na_2SO_4, evaporated under vacuum, the obtained brown residue was purified by silica gel chromatography (petroleum ether-ethyl acetate), a brown oil was obtained (3.15 g, 82 %). ^{1}H NMR ($CDCl_3$, 400 MHz) δ7.12 (d, 2H, *J* = 8.4 Hz), 6.67 (d, 2H, *J* = 8.0 Hz), 4.62 (s, 2H), 3.80 (brs, 2H), 0.91 (s, 9H), 0.08 (s, 6H).

2.2.2. N-(4-(((tert-butyldimethylsilyl)oxy)methyl)phenyl)-3-methyl-3-(2,4,5-trimethyl-3,6-dioxocyclohexa -1,4-dien-1-yl)butanamide ***3***

Compound **1** (512 mg, 2.05 mmol) was dissolved in dry CH_2Cl_2 (15 mL), to which was added N-methylmorpholine (676 μL, 6.14 mmol). The mixture was cooled to -10 ℃, an d stirred for 30 min. Then isobutyl chloroformate (311μL, 2.46 mmol) was added. After Stirring for 15 min, the solution of compound **2** (874 mg, 3.68 mmol) in dry CH_2Cl_2 was added. The resulting reaction mixture was stirred at room temperature for 12 h. The organic layer was washed with water, 5 % HCl, 5 % $NaHCO_3$, and saturated brine solution, respectively, dried over anhydrous Na_2SO_4 and filtered. The solvent was removed by a rotary evaporator, and the residue was purified by silica gel column chromatography (petroleum ether - ethyl acetate) to provide compound **3** as a yellow-brown solid (336.3 mg, 35 %). ^{1}H NMR ($CDCl_3$, 400 MHz) δ7.36 (d, 2H, *J* = 8.4 Hz), 7.28 (brs, 1H), 7.22 (d, 2H, *J* = 8.0 Hz), 4.67 (s, 2H), 3.00 (s, 2H), 2.15 (s, 3H), 1.95 (s, 6H), 1.48 (s, 6H), 0.92 (s, 9H), 0.07 (s, 6H); m. p. 101.2 - 102.4 ℃.

2.2.3. N-(4-(hydroxymethyl)phenyl)-3-methyl-3-(2,4,5-trimethyl-3,6-dioxocyclohexa-1,4-dien-1-yl) butanemide ***4***

To a solution of compound **3** (235 mg, 0.5 mmol) in methanol (20 mL) was added p-toluenesulfonic acid (PTSA) (17.2 mg, 1.0 mmol), and the reaction mixture was stirred at room temperature for 3 h. After evaporated the solvent, the residue was dissolved in CH_2Cl_2, washed with brine, dried over anhydrous

Na_2SO_4, and filtered. The crude mixture was purified by column chromatography on silica gel (petroleum ether- ethyl acetate) to afford compound **4** as a yellow solid (138 mg, 78 %). ^{1}H NMR ($CDCl_3$, 400 MHz) δ7.39 (d, 2H, *J* = 8.4 Hz), 7.27 (d, 2H, *J* = 8.0 Hz), 7.15 (s, 1H), 4.63 (s, 2H), 3.01(s, 2H), 2.15 (s, 3H), 1.94 (s, 6H), 1.49 (s, 6H). HRMS (ESI): calcd for $C_{21}H_{26}NO_4$: 356.1862; found: 356.1864 $[M+H]^+$; m. p. 144.1-145.7 ℃.

*2.2.4. 4-(3-methyl-3-(2,4,5-trimethyl-3,6-dioxocyclohexa-1,4-dien-1-yl)butanamido)benzyl(4-nitrophenyl) carbonate **5***

Compound **4** (250 mg, 0.7 mmol) was dissolved in dry CH_2Cl_2 (25 mL), and 4-nitrophenyl chloroformate (212.7 mg, 1.06 mmol) was added. To the above solution, Et_3N (106.8 mg, 1.06 mmol) was added dropwise. The resultant mixture was kept stirring for 6 h at room temperature. After completion, the reaction solution was washed with water (3 × 100 mL), dried over anhydrous Na_2SO_4. The solvent was removed, the residue was purified by column chromatography on silica gel (petroleum ether- ethyl acetate) to obtain compound **5** (305 mg, 83 %) as a yellow solid. ^{1}H NMR ($CDCl_3$, 400 MHz) δ8.27 (d, 2H, *J* = 8.0 Hz), 7.46 (d, 2H, *J* = 8.4 Hz), 7.38-7.35 (m, 4H), 7.16 (s, 1H), 5.23 (s, 2H), 3.04(s, 2H), 2.16 (s, 3H), 1.96 (s, 3H), 1.95 (s, 3H), 1.50 (s, 6H). HRMS (ESI): calcd for $C_{28}H_{28}N_2NaO_8$: 543.1743; found: 543.1746 $[M+Na]^+$; m. p. 141.7-142.6 ℃.

*2.2.5. 2-ethyl-5,5-difluoro-1,3,11-trimethyl-8-((((4-(3-methyl-3-(2,4,5-trimethyl-3,6-dioxocyclohexa-1,4-dien-1-yl)butanamido)benzyl)oxy)carbonyl)oxy)-12-phenyl-5H-pyrrolo[1',2':3,4][1,3,2]diazaborinino[1,6-a]indol-4-ium-5-uide **BOD-NQO1***

Compound **5** (93.7 mg, 0.18 mmol) and 4-dimethylaminopyridine (DMAP) (22.0 mg, 0.18 mmol) were dissolved in dry CH_2Cl_2, then added HO-BODIPY (50 mg, 0.12 mmol), and the reaction mixture was stirred for 10 h at room temperature. The reaction mixture was extracted with CH_2Cl_2 and water. The

organic layer was separated and dried over anhydrous Na_2SO_4. After the solvents was removed by rotary evaporation, the crude product was purified by silica gel column chromatography (petroleum ether-dichloromethane- ethyl acetate) to provide compound BOD-NQO1 (21 mg, 22 %) as a red solid. ^{1}H NMR ($CDCl_3$, 400 MHz) δ7.56- 7.54 (m, 4H), 7.44 (d, 2H, *J* = 8.8 Hz), 7.41 (d, 1H, *J* = 8.8 Hz), 7.36 (d, 2H, *J* = 8.4 Hz), 7.34-7.32 (m, 2H), 7.18 (s, 1H), 6.81 (dd, 1H, *J1* = 8.8 Hz , *J2* = 2.0 Hz), 5.21(s, 2H), 3.02 (s, 2H), 2.69 (s, 3H), 2.38 (q, 2H, *J* = 7.6 Hz), 2.16 (s, 3H), 1.96 (d, 6H, *J* = 2.4 Hz), 1.59 (s, 3H), 1.49 (s, 6H), 1.39 (s, 3H), 1.03 (t, 3 H, *J* = 7.6 Hz); ^{13}C NMR ($CDCl_3$, 100 MHz) δ 191.6, 187.5, 171.2, 170.3, 165.2, 153.5, 153.0, 151.5, 149.8, 148.2, 148.1, 144.3, 143.3, 142.9, 142.0, 138.3, 138.2, 138.0, 136.9, 134.9, 133.8, 130.6, 129.5, 129.4, 128.1, 121.7, 119.7, 114.9, 106.7, 69.8, 50.5, 38.4, 29.1, 17.2, 14.2, 14.1, 12.7, 12.3, 12.2, 11.1; HRMS (ESI): calcd for $C_{46}H_{46}BF_2N_3NaO_6$: 808.3345; found: 808.3352 $[M+Na]^+$; calcd for $C_{46}H_{46}BF_2N_3KO_6$: 824.3085; found: 824.3112 $[M+K]^+$; m. p. 122.8-123.5 ℃.

2.3. Preparation of Nano-NQO1 for NQO1 assay. BOD-NQO1 (0.03 mg) was poured into the micelle solution of mPEG-DSPE (6 mg) in distilled, deionised water (9 mL) under vigorous sonication for 30 min. Then the aqueous solution was filtered through a 0.22 μm polyvinylidene fluoride (PVDF) syringe driven filter and dialyzed against distilled water for 24h, and the Nano-NQO1 solution was obtained. The initial micelles solution was then diluted in PBS buffer for further studies.

3. Results and discussion

BOD-NQO1 was successfully synthesized by conjugation of HO-BODIPY and trimethyl-locked quinone propionic acid functionalized *p*-aminobenzyl alcohol through a carbonate linkage (Scheme 2). The chemical structure of BOD-NQO1 was identified by high resolution mass spectrometry (HRMS), ^{1}H NMR and ^{13}C NMR spectroscopy.

With BOD-NQO1 in hand, we initially evaluated the absorption and emission spectral changes in the

presence of a reductant under model conditions (acetonitrile/PBS buffer, 1:1, v/v, 20 mM, pH 7.4, room temperature). To improve the aqueous solubility of BOD-NQO1, acetonitrile was here chosen as a co-solvent. It should be mentioned that BOD-NQO1 only is stable for at least 48 h in the testing conditions, indicative that BOD-NQO1 is suitable for monitoring analytes in the buffer solutions (Fig. S1). As expected, the probe afforded distinct optical changes when sodium dithionite was employed as a reducing chemical. In the absence of sodium dithionite, an intensive absorption at 509 nm was noted for free BOD-NQO1 (quantum yield: 0.04). Notably, addition of sodium dithionite introduced a dramatic red-shift from 509 to 542 nm (Fig. 1A) with an obvious isosbestic point at 517 nm. The changes in the fluorescence spectra upon addition of sodium dithionite were further investigated. Time dependent fluorescence enhancement was observed with the emission wavelength red-shift from 550 nm to 575 nm (Fig. 1). These optical changes resulted from reductant triggered the lactonization and self-immolation to liberate the red fluorescent HO-BODIPY dye (Scheme 1). Dithionite initiated the production of hydroquinone, followed by a cyclic cleavage to give *p*-aminobenzyloxycarbonate. Self-immolation eventually occurred to generate the red fluorescent dye. This cascade reaction sequence was also verified by both high-performance liquid chromatography (HPLC) and high-resolution mass spectrometry (HRMS) experiments (Fig. S2). BOD-NQO1 had a HPLC retention time at 21.79 min and HRMS signal $[M + Na]^+$ at 808.3352. Likewise, the spectra of BOD-NQO1 in the presence of dithionite showed a dominant retention time at 8.94 min and peak of $[M - H]^-$ with 402.1830, identical to that of HO-BODIPY. The identity of the fluorescent product to be HO-BODIPY was further revealed ^{1}H NMR spectroscopy (Fig. S2).

It should be mentioned that BOD-NQO1 is not an ideal probe to assay the NQO1 activity, since organic solvents must be used as co-solvents to facilitate the solubility in aqueous solution. Nevertheless, organic solvents are detrimental to enzymes. Generally, small organic probes always suffer from the

limitation of low aqueous solubility. Appending hydrophilic substituents to the chromophore core is commonly employed, which requires tedious synthesis procedures. In contrast, a supramolecular assemble strategy offers an easy-to-achieve tool to afford nanoparticles with excellent aqueous solubility. Therefore, supramolecular micelle of amphiphilic polymers was explored to encapsulate BOD-NQO1 due to the establishment capability of amphiphilic building blocks assembling to form hydrophilic nanoparticles capable of entrapment hydrophobic dyes [39-41]. In this way, we constructed a nanoprobe Nano-NQO1 for interrogating the fluorescence imaging applications.

As is well known, entrapment of organic dyes with small Stokes shifts within a confined space always introduces self-quenching of fluorescence behaviour [34]. Thus, we systematically investigated the effects of encapsulating amount of BOD-NQO1 on the fluorescence of Nano-NQO1. In general, the amount of the encapsulated BOD-NQO1 can be fine-tuned in a broad range. As shown in Fig. S3, the change of the loading amount induced varied fluorescence intensity, and relatively strong emission could be obtained when the ratio BOD-NQO1/ mPEG-DSPE was empirically optimized as 0.004−0.02 by weight. In the optimized entrapment protocol, the ratio of BOD-NQO1/ mPEG-DSPE is about 0.005 at pH 7.4. The morphologies and hydrodynamic size of Nano-NQO1 were then determined by transmission electron microscopy and dynamic light scattering, respectively. The as-prepared nanoparticles are uniform with an average hydrodynamic size of 25 nm, which was in accordance with the diameters given by TEM (Fig. S4). Besides, the photo- and chemical stability of Nano-NQO1 was tested (Fig. S5). No obvious changes in absorption and emission spectra were observed after storage for 48 h. Good photostability was also revealed by continuous irradiation with an Hg/Xe lamp for 2 h, during which time only a minimal change minimal change was observed in the optical spectra. Overall, the outstanding stability and good aqueous solubility endow superiority of Nano-NQO1 in bioimaging.

We next evaluated the fluorescence changes of Nano-NQO1 toward a reducing reagent in PBS buffer. Fig. S6 represents the time-dependent fluorescence spectral changes upon addition of 1 mM sodium dithionite. Gratifyingly, dithionite elicited a distinct ratiometric fluorescence change identified by the observation of a gradual increase in the emission intensity at 585 nm and a concomitant loss of emission at 550 nm. Obviously, this remarkable ratiometric fluorescence signal change arose from reductant-promoted conversion of BOD-NQO1 to HO-BODIPY within the hydrophobic interior of micellar assembly. After the successful demonstration of Nano-NQO1 as a suitable ratiometric fluorescent probe for sensing reducing reagent, we sought to establish this newly designed nanoprobe is indeed promising fluorescent probe capable of NQO1 activity assay. As shown in Fig. 2A, in the absence of NQO1, Nano-NQO1 displayed a relatively weak emission band at 550 nm. Upon incubation with NQO1, the emission maximum at 550 nm underwent a reduction accompanied by a remarkable fluorescence enhancement at 585 nm. An obvious isoemission point was also noted at 557 nm. Obviously, the reaction rate between Nano-NQO1 and NQO1 is slower than that of Nano-NQO1 with $Na_2S_2O_4$. This result can be ascribed to the fact that the steric hindrance of the biomacromolecule NQO1 limited its free accessibility to BOD-NQO1 located in the core of the assemblies [12]. It is worth mentioning that the fluorescence intensity ratio of the two emission bands at 550 and 585 nm (I_{585}/I_{550}) increased from 0.7 to 2.5 as the incubation time proceeded (Fig. 2B), showing a 3-fold enhancement factor, which allowed the assay of NQO1 activity by an efficient ratiometric fluorescence mode. In contrast, minimal ratiometric fluorescence change was observed by pretreatment of NQO1 with dicoumarol (3,3'-methylene-bis(4-hydroxycoumarin)), a commonly used inhibitor of NQO1, confirming the key role of NQO1 in introducing the ratiometric fluorescence signal change (Fig.

2B, Fig. S7). The kinetic values of Nano-NQO1 against NQO1 were subsequently determined by incubating NQO1 with Nano-NQO1 in PBS buffer at 37 ℃ (Fig. 2C). According to Michaelis–Menten equation, the K_m and V_{max} values were then calculated to be 6.77 μM and 0.043 μM min^{-1}, respectively (Fig.S8).

Nano-NQO1 afforded good selectivity for NQO1 over other related species when utilizing I_{585}/I_{550} as the detection signals. As shown in Fig. 3, when other species such as phosphatase, aprotinin, collagenase□, lipase, glucoamylase, 10% FBS, 10% human plasma were incubated with Nano-NQO1 in the presence of 500 μM NADH, minimal fluorescence changes were noted.

After demonstration of the promising responsive behavior of Nano-NQO1 for specific monitoring the NQO1 activity, we then explored the ratiometric characteristic of Nano-NQO1 for evaluation of enzyme activity in living cells (Fig. 4 and Fig. S9). Since HT-29 cells are known to show high NQO1 activity and H596 cells are identified to have negligible NQO1 activity, here HT-29 cells and H596 cells were explored as NQO1-positive and NQO1-negative model cell systems, respectively. HT-29 cells incubated with NaNo-NQO1 for 30 minutes gave moderate fluorescence signals in both green channel and red channel. The ratio of the two images generated from red to green channel is estimated to be about 0.8 (Fig. 4A). As the incubation time increases, the image ratio enhanced to be 2 (Fig. 4B). Such time-dependent ratio change can be attributed to NQO1-induced reduction of Nano-NQO1. In sharp contrast, no time-dependent ratio enhancement was observed upon incubation with NQO1-negative H596 cells. When H596 cells were treated with Nano-NQO1 for 30 min (Fig. 4C) and 120 min (Fig. 4D), the image ratio remained constant value at about 0.6, inferring no occurrence of reduction. These results indicate that Nano-NQO1 can serve as an efficient tool for differentiating NQO1-positive cancer cells from

NQO1-negative cells. An enzyme inhibition test was then performed to validate that the obtained imaging signal indeed derived from NQO1 activity. When HT-29 cells were pretreated with various concentrations of dicoumarol and followed by incubation with Nano-NQO1 for 120 minutes, the ratio was greatly reduced when compared to that without dicoumarol (Fig. 4B). As shown in Fig. 4E-F, with increasing the concentration of dicoumarol from 0 to 1 mM, the fluorescence ratio from red to green channel ultimately decreased to be 1. Collectively, Nano-NQO1 possesses the capability of differentiating NQO1-expressing and NQO1-nonexpressing cancer cell via the preferable ratiometric measurement of NQO1 activity.

4. Conclusion

In summary, we report the polymeric micelle assembly based nanoprobes for ratiometric monitoring cancer-specific NQO1. To this end, we firstly designed a small molecule probe BOD-NQO1, wherein reductant can mediate cascade reactions to deliver the red fluorescent 6-hydroxylphenol-BODIPY dye. Unfortunately, the poor solubility of BOD-NQO1 in aqueous solution seriously retards its direct assay of NQO1 activity. Encapsulation of BOD-NQO1 within the hydrophobic interior of a polymeric micelle assembly was then employed to create a nanoprobe with excellent aqueous solubility, significantly enhanced chemical and photo-stability as well as biocompatibility. Satisfyingly, such nanoprobe possesses the capability of differentiating NQO1-positive cancer cells from NQO1-negative cells via the preferable ratiometric measurement of NQO1 activity. We expect that the present design strategy would benefit the establishment of versatile fluorescence probes for practical assay of cancer biomarkers.

Acknowledgements

We gratefully acknowledge the financial support by the National Science Foundation of China (grant numbers 21172071, 21190033, 21372083), National 973 Program (2013CB733700) and the Programme

of Introducing Talents of Discipline to Universities (B16017).

References

[1] Blum G, Von Degenfeld G, Merchant M J, Blau H M, Bogyo M. Noninvasive optical imaging of cysteine protease activity using fluorescently quenched activity-based probes. Nat Chem Biol 2007; 3: 668-77.

[2] Bremer C, Tung C-H, Weissleder R. In vivo molecular target assessment of matrix metalloproteinase inhibition. Nat Med 2001; 7: 743-8.

[3] Wang X, Hu J, Zhang G, Liu S. Highly selective fluorogenic multianalyte biosensors constructed via enzyme-catalyzed coupling and aggregation-induced emission. J Am Chem Soc 2014; 136: 9890-3.

[4] Chang J W, Moellering R E, Cravatt B, F. An activity-based imaging probe for the integral membrane hydrolase KIAA1363. Angew Chem Int Ed 2012; 51: 966-70.

[5] Myochin T, Hanaoka K, Komatsu T, Terai T, Nagano T. Design strategy for a near-infrared fluorescence probe for matrix metalloproteinase utilizing highly cell permeable boron dipyrromethene. J Am Chem Soc 2012; 134: 13730-7.

[6] Mizukami S, Takikawa R, Sugihara F, Shirakawa M, Kikuchi K. Dual-function probe to detect protease activity for fluorescence measurement and ^{19}F MRI. Angew Chem Int Ed 2009; 48: 3641-3.

[7] Fujikawa Y, Urano Y, Komatsu T, Hanaoka K, Kojima H, Terai T, et al. Design and synthesis of highly sensitive fluorogenic substrates for glutathione s-transferase and application for activity imaging in living cells. J Am Chem Soc 2008; 130: 14533-43.

[8] Wu J, Liang D, Jin Q, Liu J, Zheng M, Duan X, Tang X. Bioorthogonal SERS Nanoprobes for Mulitplex Spectroscopic Detection and Tumor Cell Targeting and Tissue Imaging, Chem. Eur. J., 2015; 21: 12914-8..

[9] Shi H, Kwok R T K, Liu J, Xing B, Tang B Z, Liu B. Real-time monitoring of cell apoptosis and drug screening using fluorescent light-up probe with aggregation-induced emission characteristics. J Am Chem Soc 2012; 134: 17972-81.

[10] Rao J, Hottinger C, Khan A. Enzyme-triggered cascade reactions and assembly of abiotic block copolymers into micellar nanostructures. J Am Chem Soc 2014; 136: 5872-5.

[11] Xie H X, Mire J, Kong Y, Chang M H, Hassounah H A, Thornton C N, et al. Rapid point-of-care detection of the tuberculosis pathogen using a BlaC-specific fluorogenic probe. Nat Chem 2012; 4: 802-9.

[12] Ding Y, Kang Y, Zhang X. Enzyme-responsive polymer assemblies constructed through covalent synthesis and supramolecular strategy. Chem Commun 2015; 51: 996-1003.

[13] Ye D, Liang G, Ma M L, Rao J. Controlling intracellular macrocyclization for the imaging of protease activity. Angew Chem Int Ed 2011; 50: 2275-9.

[14] Li L, Ge J, Wu H, Xu Q-H, Yao S Q. Organelle-specific detection of phosphatase activities with two-photon fluorogenic probes in cells and tissues. J Am Chem Soc 2012; 134: 12157-67.

[15] Östman A, Hellberg C, Böhmer F D. Protein-tyrosine phosphatases and cancer. Nat Rev Cancer 2006; 6: 307-20.

[16] Razgulin A, Ma N, Rao J. Strategies for in vivo imaging of enzyme activity: an overview and recent advances. Chem Soc Rev 2011; 40: 4186-216.

[17] Urano Y, Sakabe M, Kosaka N, Ogawa M, Mitsunaga M, Asanuma D, et al. Rapid cancer detection by topically spraying a γ-glutamyltranspeptidase-activated fluorescent probe. Sci Transl Med 2011; 3: 110ra119.

[18] Wang F, Zhu Y, Zhou L, Pan L, Cui Z, Fei Q, et al. Fluorescent in situ targeting probes for rapid

imaging of ovarian-cancer-specific γ-glutamyltranspeptidase. Angew Chem In Ed 2015; 54: 7349-53.

[19] Li L, Shi W, Wang Z, Gong Q, Ma H. Sensitive fluorescence probe with long analytical wavelengths for γ-glutamyl transpeptidase detection in human serum and living cells. Anal Chem 2015; 87: 8353-9.

[20] Zhang H, Fan J, Wang J, Dou B, Zhou F, Cao J, et al. Fluorescence discrimination of cancer from inflammation by molecular response to COX-2 enzymes. J Am Chem Soc 2013; 135: 17469-75.

[21] Zhang H, Fan J, Wang J, Zhang S, Dou B, Peng X. An off-on COX-2-specific fluorescent probe: targeting the golgi apparatus of cancer cells. J Am Chem Soc 2013; 135: 11663-9.

[22] Gehrig S, Mall M A, Schultz C. Spatially resolved monitoring of neutrophil elastase activity with ratiometric fluorescent reporters. Angew Chem Int Ed 2012; 51: 6258-61.

[23] Sakabe M, Asanuma D, Kamiya M, Iwatate R J, Hanaoka K, Terai T, et al. Rational design of highly sensitive fluorescence probes for protease and glycosidase based on precisely controlled spirocyclization. J Am Chem Soc 2013; 135: 409-14.

[24] Li Y, Sun Y, Li J, Su Q, Yuan W, Dai Y, et al. Ultrasensitive near-infrared fluorescence-enhanced probe for in vivo nitroreductase imaging. J Am Chem Soc 2015; 137: 6407-16.

[25] Li Z, Li X, Gao X, Zhang Y, Shi W, Ma H. Nitroreductase detection and hypoxic tumor cell imaging by a designed sensitive and selective fluorescent probe, 7-[(5-Nitrofuran-2-yl) methoxy]-3 H-phenoxazin-3-one. Anal Chem 2013; 85: 3926-32.

[26] Belinsky M, Jaiswal A K. NAD (P) H: Quinone oxidoreductase1 (DT-Diaphorase) expression in normal and tumor tissues. Cancer Metastasis Rev 1993; 12: 103-117.

[27] Pink J J, Planchon S M, Tagliarino C, Varnes M E, Siegel D, Boothman D A. NAD (P) H: quinone oxidoreductase activity is the principal determinant of β-lapachone cytotoxicity. J Bio Chem 2000;

275: 5416-24.

[28] Bey E A, Bentle M S, Reinicke K E, Dong Y, Yang C-R, Girard L, et al. An NQO1-and PARP-1-mediated cell death pathway induced in non-small-cell lung cancer cells by β-lapachone. Proc Natl Acad Sci USA 2007; 104: 11832-7.

[29] Ma X, Huang X, Huang G, Li L, Wang Y, Luo X, et al. Prodrug strategy to achieve lyophilizable, high drug loading micelle formulations through diester derivatives of β-lapachone. Adv Healthcare Mater 2014; 3: 1210-6.

[30] Silvers W C, Prasai B, Burk D H, Brown M L, McCarley R L. Profluorogenic reductase substrate for rapid, selective, and sensitive visualization and detection of human cancer cells that overexpress NQO1. J Am Chem Soc 2013; 135: 309-14.

[31] Hettiarachchi S U, Prasai B, McCarley R L. Detection and cellular imaging of human cancer enzyme using a turn-on, wavelength-shiftable, self-immolative profluorophore. J Am Chem Soc 2014; 136: 7575-8.

[32] Silvers W C, Payne A S, McCarley R L. Shedding light by cancer redox-human NAD (P) H: quinone oxidoreductase 1 activation of a cloaked fluorescent dye. Chem Commun 2011; 47: 11264-6.

[33] Prasai B, Silvers W C, McCarley, R L. Oxidoreductase-facilitated visualization and detection of human cancer cells. Anal Chem 2015; 87: 6411-8.

[34] Zhao C, Zhang X, Li K, Zhu S, Guo Z, Zhang L, et al. Förster resonance energy transfer switchable self-assembled micellar nanoprobe: ratiometric fluorescent trapping of endogenous H_2S generation via fluvastatin-stimulated upregulation. J Am Chem Soc 2015; 137: 8490-8.

[35] Niu L-Y, Chen Y-Z, Zheng H-R, Wu L-Z, Tung C-H, Yang Q-Z. Design strategies of fluorescent probes for selective detection among biothiols. Chem Soc Rev 2015; 44: 6143-60.

[36] Yang Y, Zhao Q, Feng W, Li F. Luminescent chemodosimeters for bioimaging. Chem Rev 2013; 113: 192-270.

[37] Li L, Yuzhuo, Tang X. Quaternary Ammonium Promoted Ultra Selective and Sensitive Fluorescence Detection of Fluoride Ion in Water and Living Cells, Anal. Chem., 2014; 86: 10006-9.

[38] Zhang L, Zhu H, Li M, Gu X. A novel fluorescent probe for imaging endogenous hydrogen sulphide via the CSE enzymatic pathway. Chem Commun 2015; 51: 13135-7.

[39] Hu J M, Liu S Y. Engineering responsive polymer building blocks with host-guest molecular recognition for functional applications. Acc Chem Res 2014; 47: 2084-95.

[40] Li K, Qin W, Ding D, Tomczak N, Geng J, Liu R, et al. Photostable fluorescent organic dots with aggregation-induced emission (AIE Dots) for noninvasive long-term cell tracing. Sci Report 2013; 3: 1150.

[41] Peng H-Q, Niu L-Y, Chen Y-Z, Wu L-Z, Tung C-H, Yang Q-Z. Biological applications of supramolecular assemblies designed for excitation energy transfer. Chem Rev 2015; 115: 7502-42.

[42] Borchardt R T, Cohen L A. Stereopopulation control. III. facilitation of intramolecular conjugate addition of the carboxyl group. J Am Chem Soc 1972; 94: 9175-82.

[43] Zhao C, Li X, Yang Y, Cao J, Wang X, Zhang Y. Construction of BODIPY-CTAB assembles for ratiometric fluorescence pH measurements in complete water system. Dyes Pigm 2014; 101: 130-135.

Figure Captions

Fig. 1. Time dependent spectra changes of BOD-NQO1 (10 μM) in the presence of 5 mM $Na_2S_2O_4$ under model conditions (acetonitrile/PBS buffer, 1:1, v/v, 20 mM, pH 7.4, room temperature), (A) absorption, (B) fluorescence; and (C) Time dependent fluorescence intensity changes at 575 nm.

Fig. 2. (A) Time dependent fluorescence spectra changes of Nano-NQO1 (1.1 mg/mL, 10 μM BOD-NQO1) in the presence of NQO1 (80 μg) and NADH (500 μM); (B) the ratiometric fluorescence intensity changes of Nano-NQO1 + NQO1 (80 μg) + NADH (500 μM) in the absence and presence of dicoumarol (1 mM) in PBS (pH 7.4) containing 0.007% bovine serum albumin (BSA) at 37 ℃. (C) Kinetic course of Nano-NQO1 in the presence of NQO1 (80 μg) in PBS (pH 7.4) containing 0.007% BSA at 37 ℃; Solid red line represents best fit to Michaelis–Menten equation. Here, the concentration of Nano-NQO1 (mg/mL) was converted to that of BOD-NQO1 (μM) when calibrating the plot, thus the obtained plot can be used for comparison with the reported ones. λ_{ex} = 510 nm.

Fig. 3. Time-dependent ratiometric fluorescence changes of Nano-NQO1 (10 μM BOD-NQO1) toward various substrates in PBS (pH 7.4) at 37 ℃. λ_{ex} = 510 nm. These analytes of interest contain phosphatase, aprotinin, collagenase Ⅰ, lipase, glucoamylase, 10% FBS, 10% human plasma, nitroreductase (NTR) and NQO1.

Fig. 4. Confocal microscopy images of HT-29 (NQO1-positive) (A, B), H596 (NQO1-negative) (C, D) cells, HT-29 cells in the presence of dicoumarol 0.2 mM (E), 1 mM (F), λex = 514 nm, the emission was collected at 520–560 nm (assigned to green channel) and 570–610 nm (red channel), ratio image generated from red to green channel: A and C) cells were incubated with Nano-NQO1 (1.1 mg/mL) for 30 min; B, D, E, F for 120 min.

Scheme 1. Schematic representations of reductant-mediated cascade reactions in conversion of

BOD-NQO1 to HO-BODIPY and polymeric micelle assembly for facile access to nanoprobes with ratiometric response to NQO1.

Scheme 2. Synthetic route for BOD-NQO1.

Figures

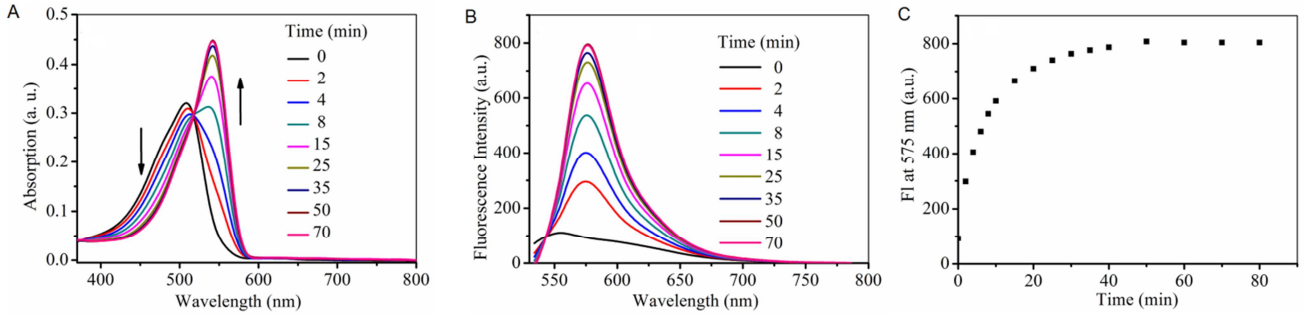

Fig. 1

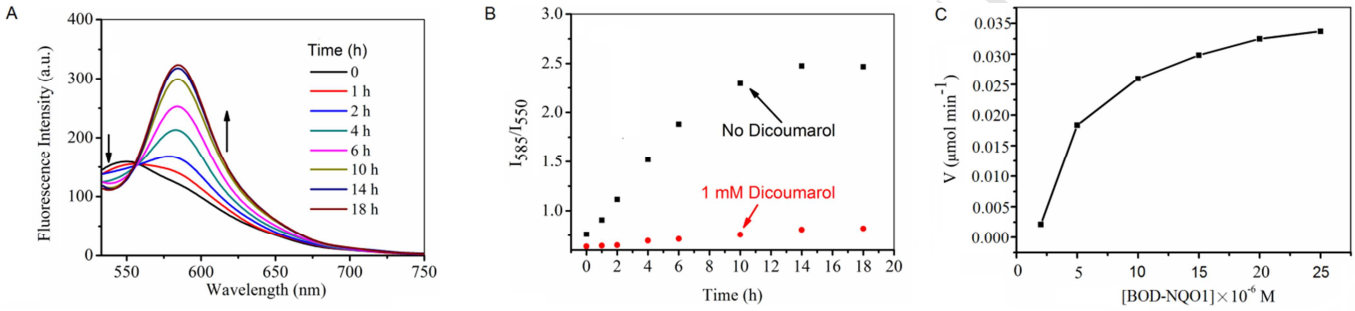

Fig. 2

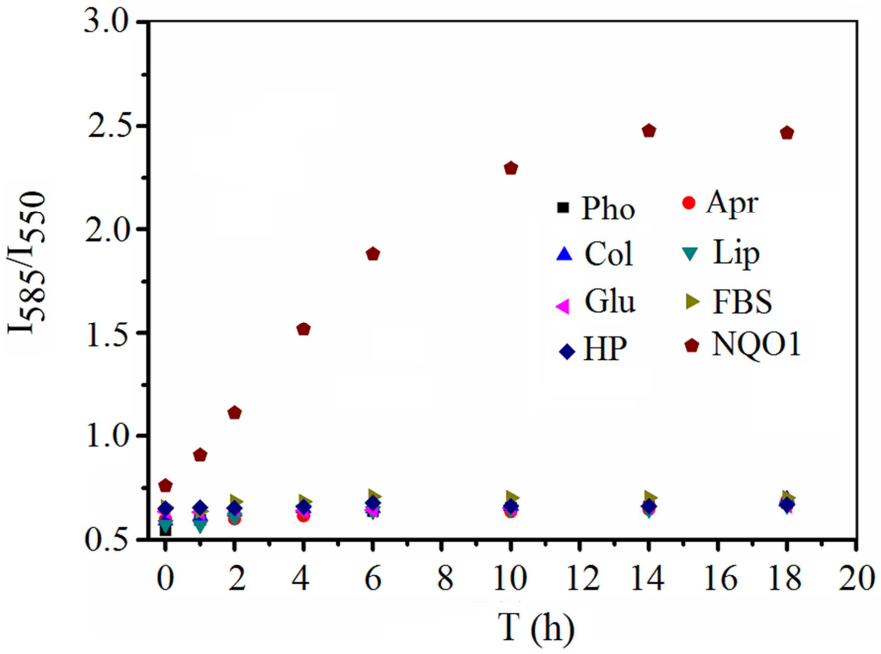

Fig. 3

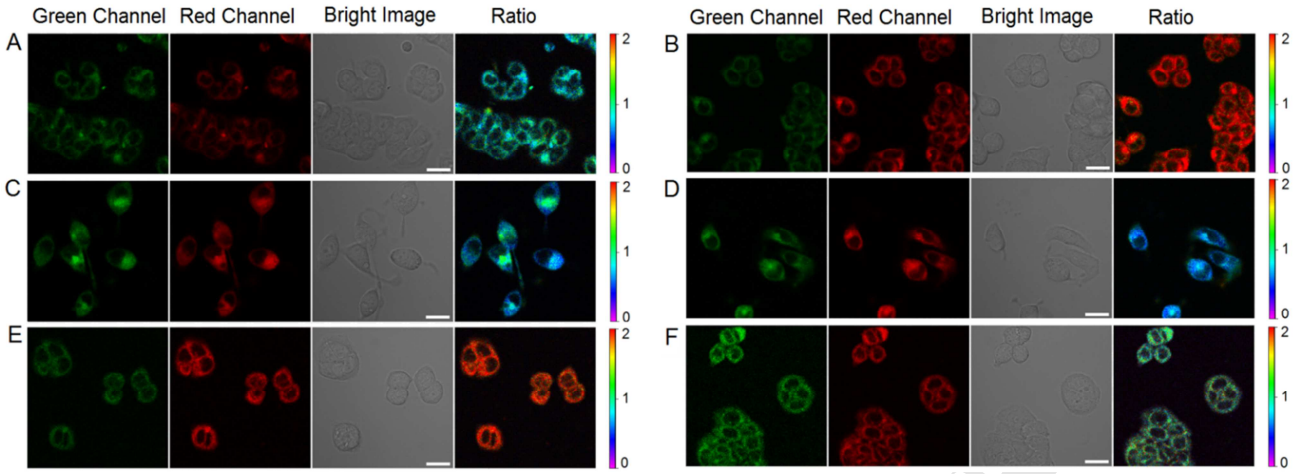

Fig. 4

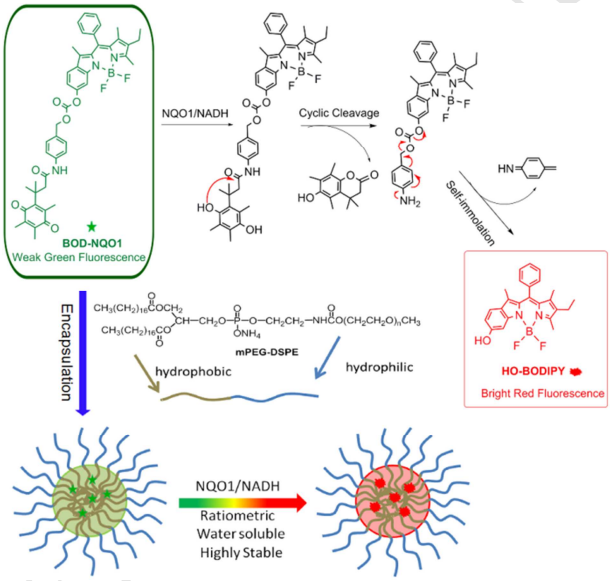

Scheme 1.

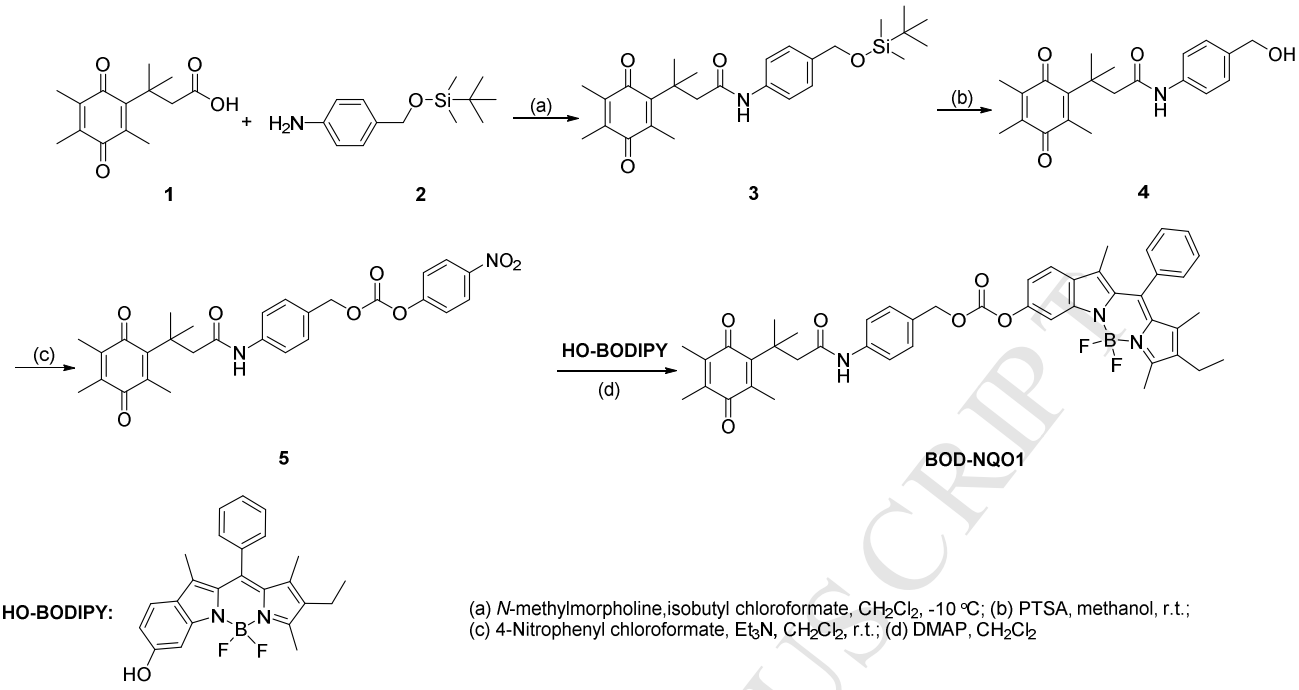

Scheme 2.

Rational Construction of Probes Rendering Ratiometric Response to the Cancer-Specific Enzyme NQO1

Qiang Fei,[†,‡] Li Zhou,[#] Feiyi Wang,[‡] Ben Shi,[‡] Chunbao Li,[*,†] Rui Wang,[#] He Tian,[‡] Chunchang Zhao*[,‡]

† Department of Chemistry, School of Science, Tianjin University, Tianjin 300072 (China), E-Mail: lichunbao@tju.edu.cn

‡ Key Laboratory for Advanced Materials and Institute of Fine Chemicals, East China University of Science & Technology, Shanghai 200237 (China)

E-mail: zhaocchang@ecust.edu.cn

Shanghai Key Laboratory of New Drug Design, School of Pharmacy, East China University of Science & Technology, Shanghai 200237 (P. R. China.)

1. Cells culture and imaging. HT-29 cells were cultured in McCoy's 5A medium supplemented with 10 % fetal bovine serum (FBS) at 37 ℃ in a humidified a tmosphere of 5/95 CO_2/air incubator.

For fluorescence imaging, cells were incubated in glass bottom dishes and stabilized for 24 h. For imaging HT-29 cells, the cells were incubated with Nano-NQO1 (1.1 mg/mL) for 30 min and 120 min, respectively, subsequently the cells were washed three times with PBS. Then, the confocal imaging was performed using Nikor AIR with a 60 × oil objective. The excitation wavelength was at 514 nm, the emission was collected at 520-560 nm for green fluorescence and emission at 570-610 nm for red channel.

The same procure was applied to H596 cells with the exception of using Roswell Park Memorial Institute 1640 medium (RPMI-1640) as the culture medium.

In inhibition assay, the cells were incubated with various concentrations of dicoumarol prior to treatment with Nano-NQO1.

2. Chemical stability of BOD-NQO1 in testing buffer solution.

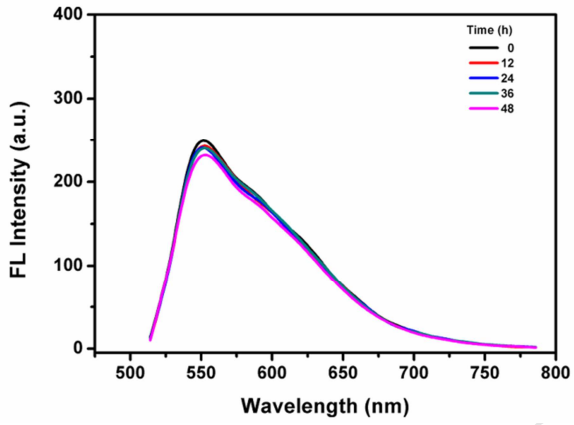

Fig. S1. Chemical stability of BOD-NQO1 in PBS-CH_3CN (V/V, 1:1) determined by time dependent fluorescence spectra changes.

3. Identification of the product by HPLC and HRMS.

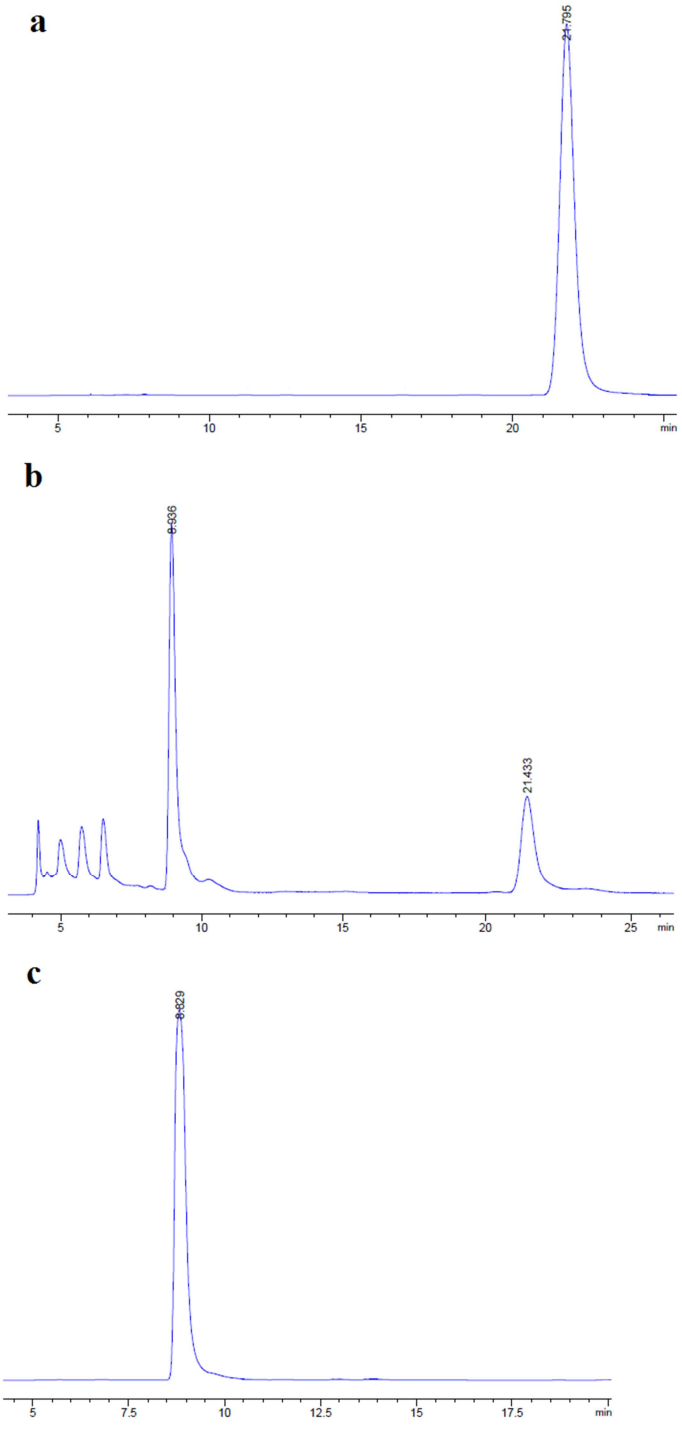

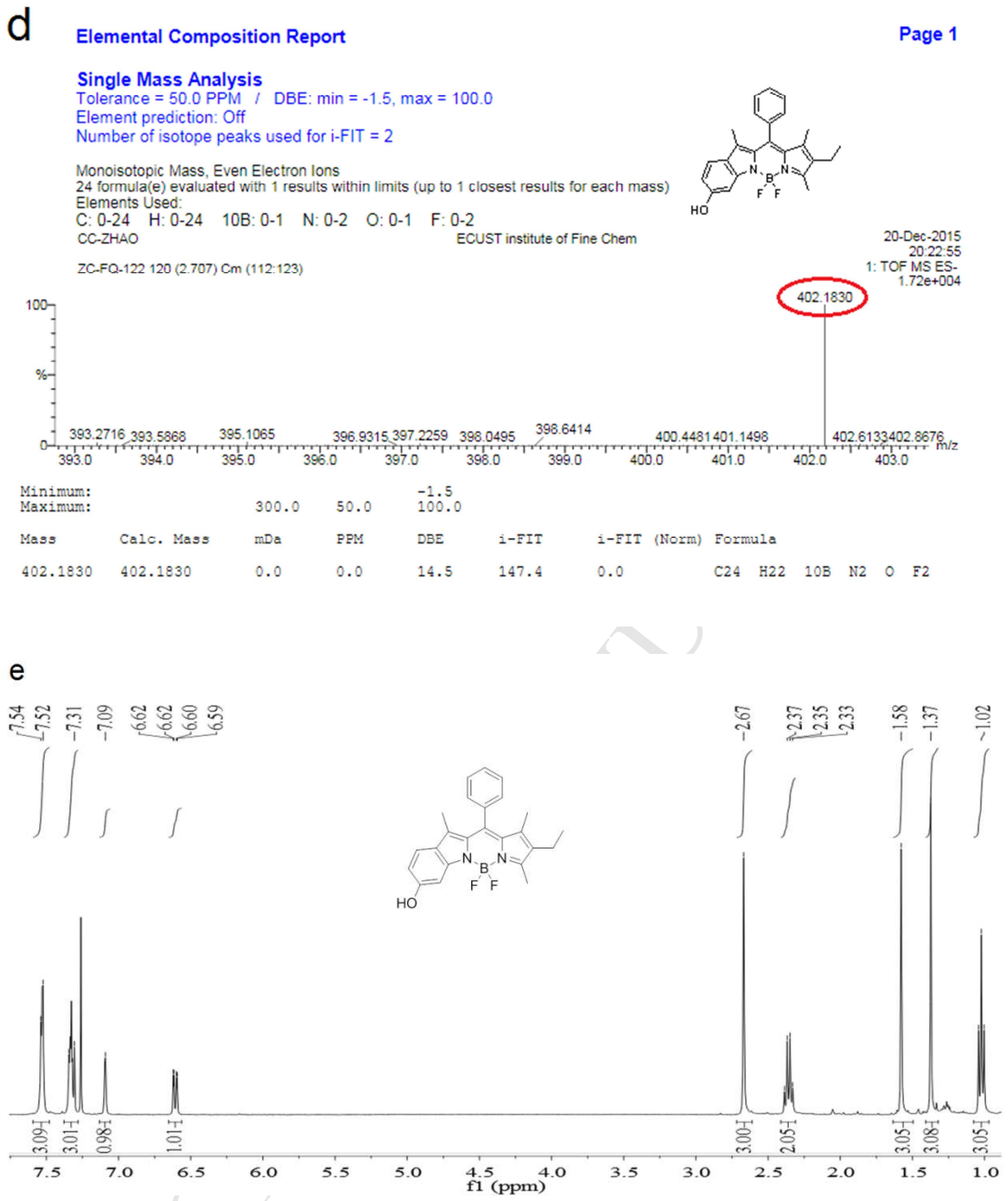

Fig. S2 HPLC profiles of (a) BOD-NQO1, (b) BOD-NQO1 + $Na_2S_2O_4$, (c) HO-BODIPY. HPLC was carried out on a ZORBAX 80A Extend-C18 column (4.6 × 250 mm, 5 μm, Agilent). The conditions were as follows: volume ratio of acetonitrile/H_2O = 90:10; flow rate is 0.5 mL·min^{-1}; detection under UV light at 509 nm and 542 nm. (d) High-resolution mass spectrometry of HO-BODIPY. (e) ^{1}H NMR spectrometry of the fluorescent product of BOD-NQO1 + $Na_2S_2O_4$.

4. The effects of encapsulating amount of BOD-NQO1 on the fluorescence.

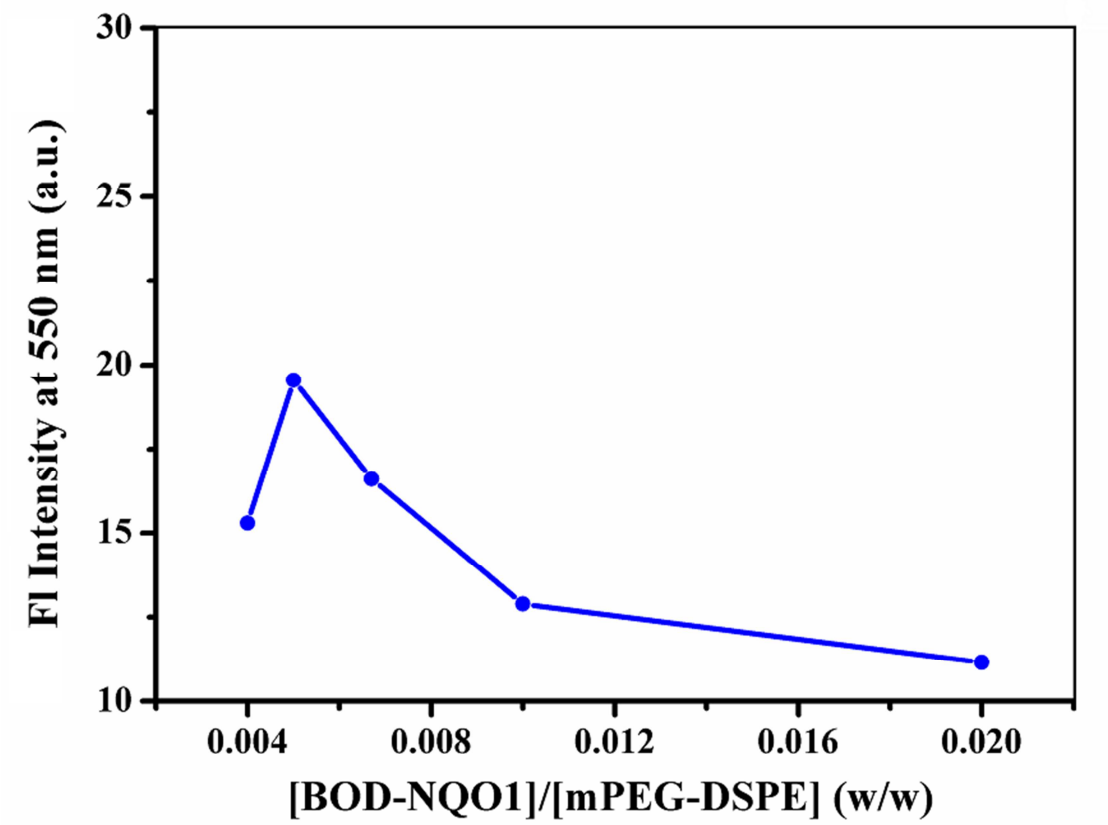

Fig. S3 The effects of encapsulating amount of BOD-NQO1 in mPEG-DSPE (6 mg) on the fluorescence.

5. The morphologies and hydrodynamic size of Nano-NQO1.

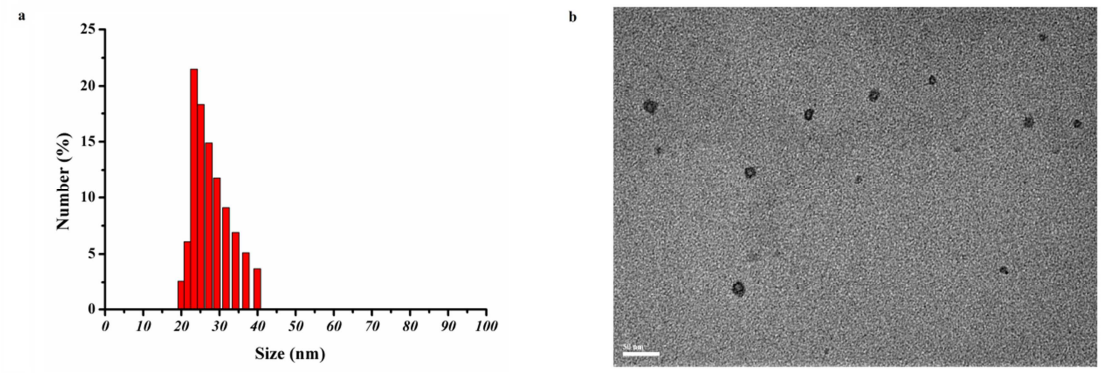

Fig. S4 a) Average hydrodynamic size of Nano-NQO1 as determined by dynamic light scattering; b) Representative TEM image of Nano-NQO1, the scale bar is 50 nm.

Note: The average hydrodynamic size of Nano-NQO1 is about 25 nm as determined by dynamic light scattering and transmission electron microscopy.

6. Stability of Nano-NQO1.

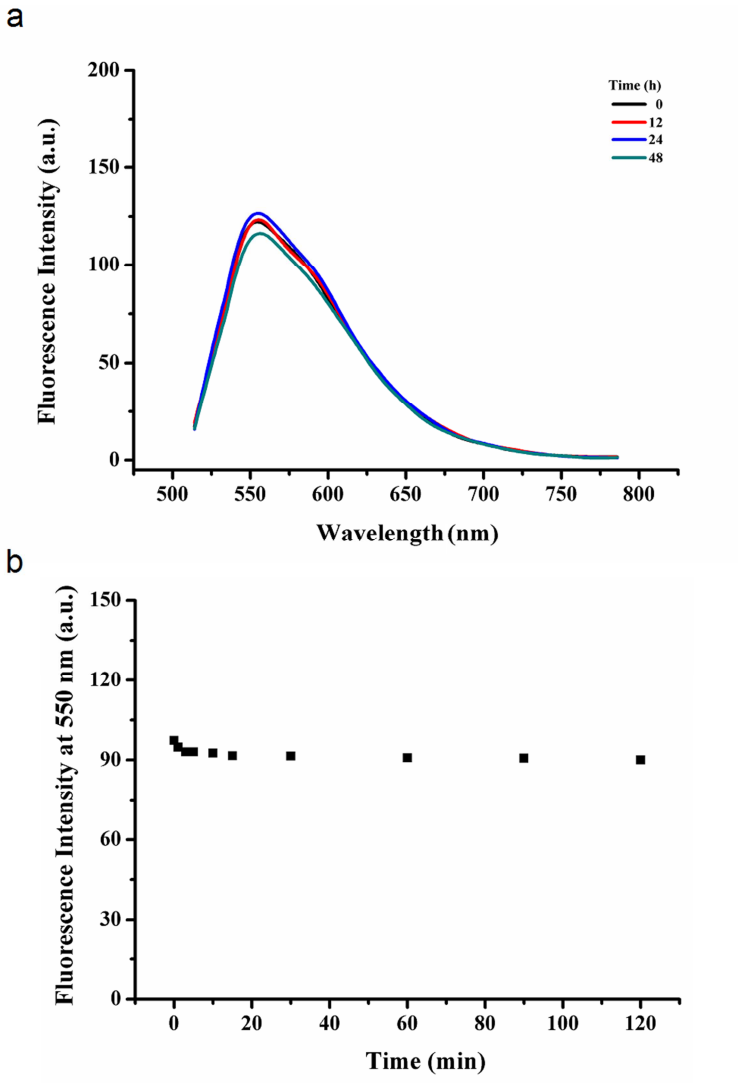

Fig. S5 Stability of Nano-NQO1. a) Time dependent fluorescence spectra in PBS buffer; b) Time course of fluorescence intensity change of Nano-NQO1 at 550 nm under continuous irradiation with an Hg/Xe lamp (Hamamatsu, LC8 Lightningcure, 150 W).

7. Fluorescence spectra changes of Nano-NQO1 upon addition of $Na_2S_2O_4$.

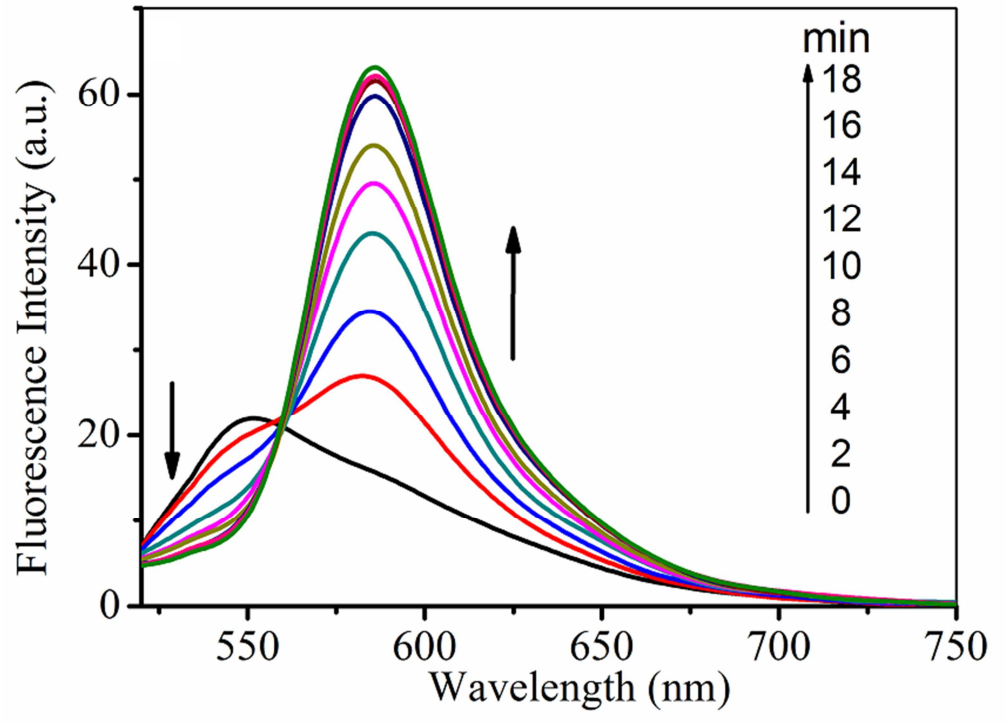

Fig. S6 Time dependent fluorescence spectra changes of Nano-NQO1 (10 μM BOD-NQO1) in the presence of $Na_2S_2O_4$ (1 mM) in PBS (pH 7.4) at room temperature.

8. The influence of dicoumarol.

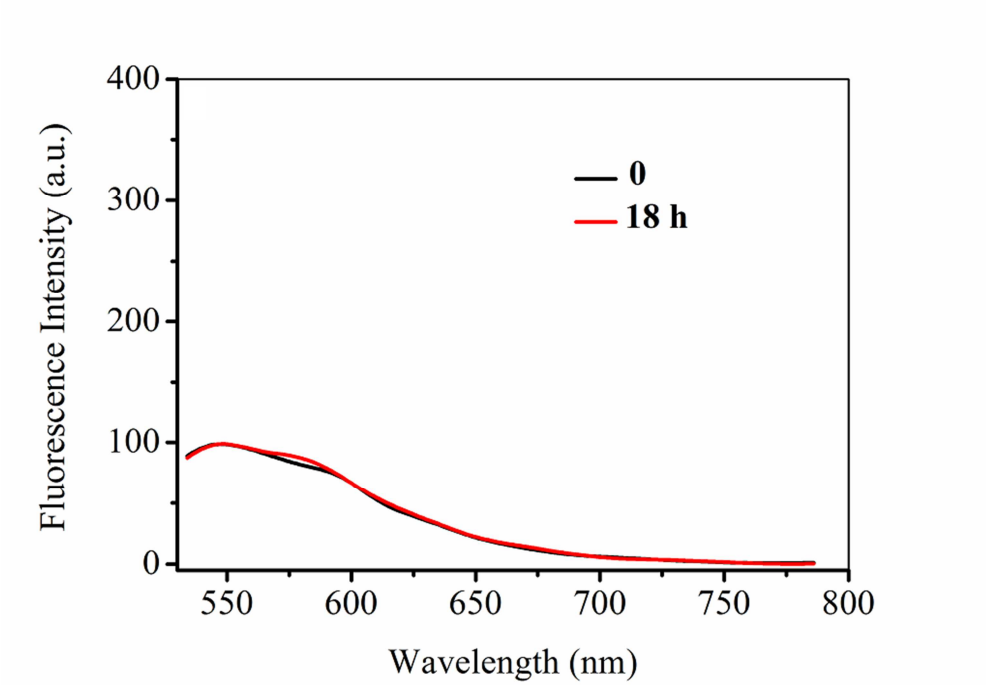

Fig. S7 Time dependent fluorescence spectra of Nano-NQO1 (10 μM BOD-NQO1) + NQO1 (80 μg) + NADH (500 μM) + dicoumarol (1 mM) in PBS (pH 7.4) at 37 ℃.

9. Correlation between 1/V and [Nano-NQO1].

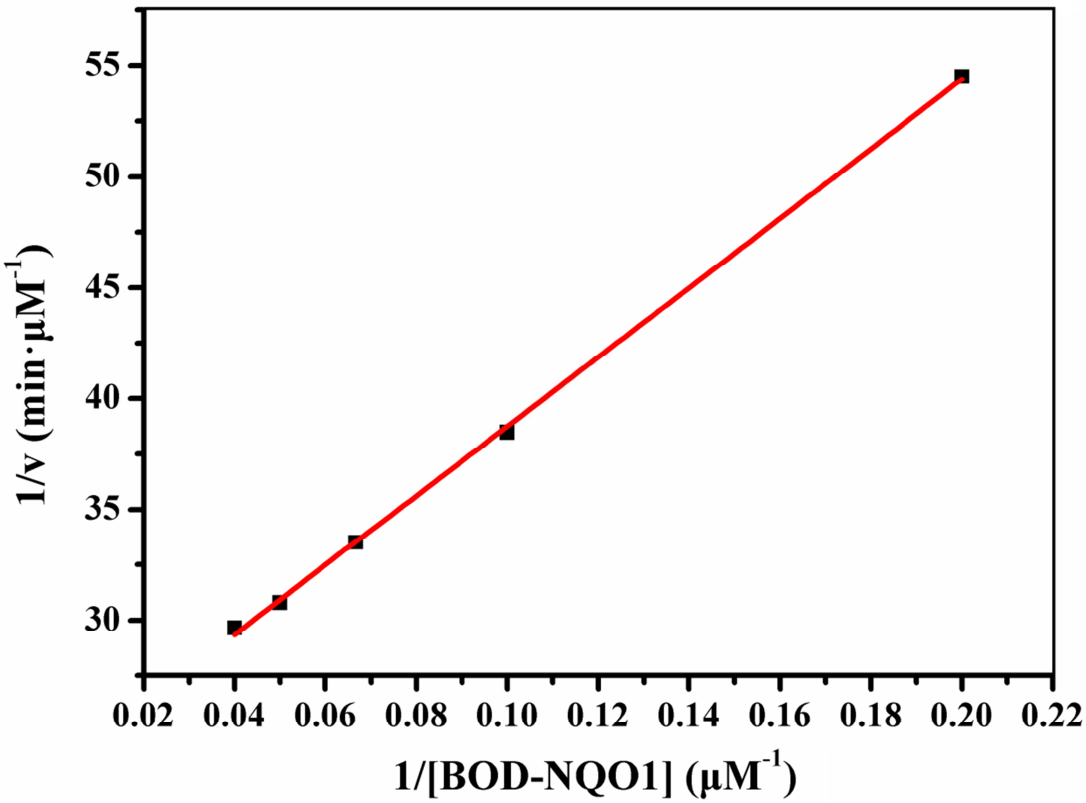

Fig. S8 Linear correlation between 1/V and Nano-NQO1 concentrations. The equation $1/V = (K_m/V_{max}) \times (1/[\text{Nano-NQO1}]) + 1/V_{max}$ can be deduced according to Michaelis-Menten equation $V = V_{max} \times [\text{Nano-NQO1}]/(K_m + [\text{Nano-NQO1}])$, where V is the velocity and [Nano-NQO1] is the concentration, K_m is the Michaelis constant. From the linear plot, the slope and the intercept can be obtained, then K_m, V_{max} were determined to be 6.77 μM and 0.043 μM min^{-1}, respectively. It should be noted that we here converted the concentration of Nano-NQO1 (mg/mL) to that of BOD-NQO1 (μM) in calibrating the plot according to Beer-Lambert Law, thus the obtained values of K_m and V_{max} have units of μM and μM min^{-1}, which can be used for comparison with the reported data.

10. Confocal microscopy images of HT-29 and H596 cells.

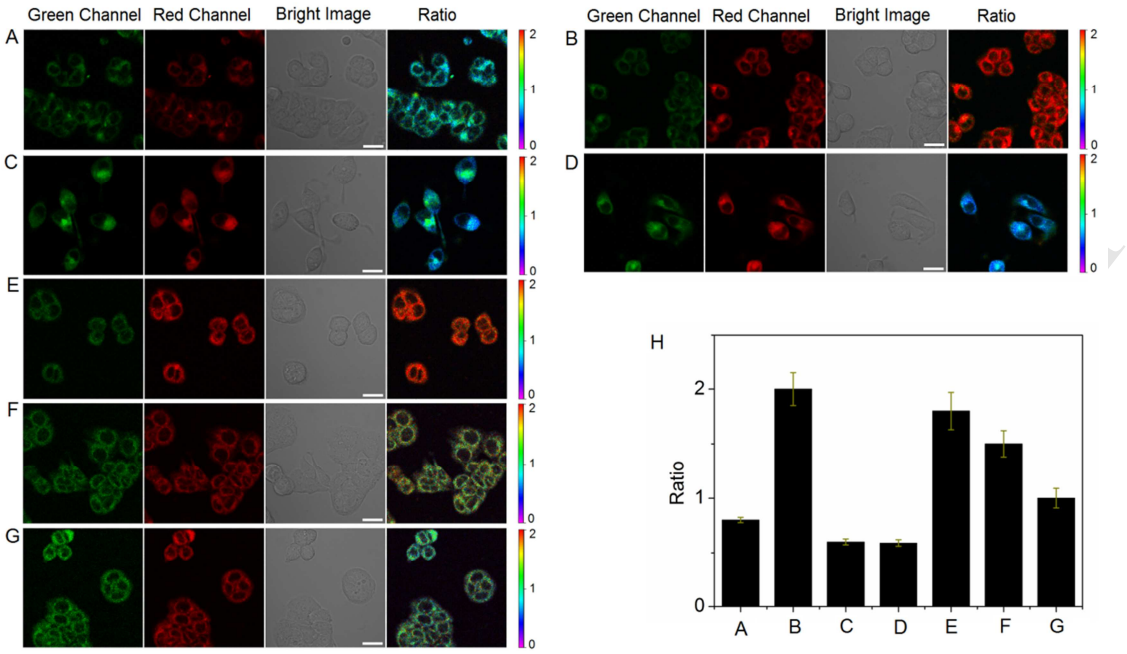

Fig. S9 Confocal microscopy images of HT-29 (NQO1-positive) (A, B), H596 (NQO1-negative) (C, D) cells, HT-29 cells in the presence of dicoumarol 0.2 mM (E), 0.5 mM (F), 1 mM (G), λex = 514 nm, the emission was collected at 520–560 nm (assigned to green channel) and 570–610 nm (red channel), ratio image generated from red to green channel: A and C) cells were incubated with Nano-NQO1 (1.1 mg/mL) for 30 min; B, D, E, F and G) for 120 min. (H) The image ratio values estimated from red to green channel. Scale bar represents 20 μm.

11. NMR and HRMS spectra.

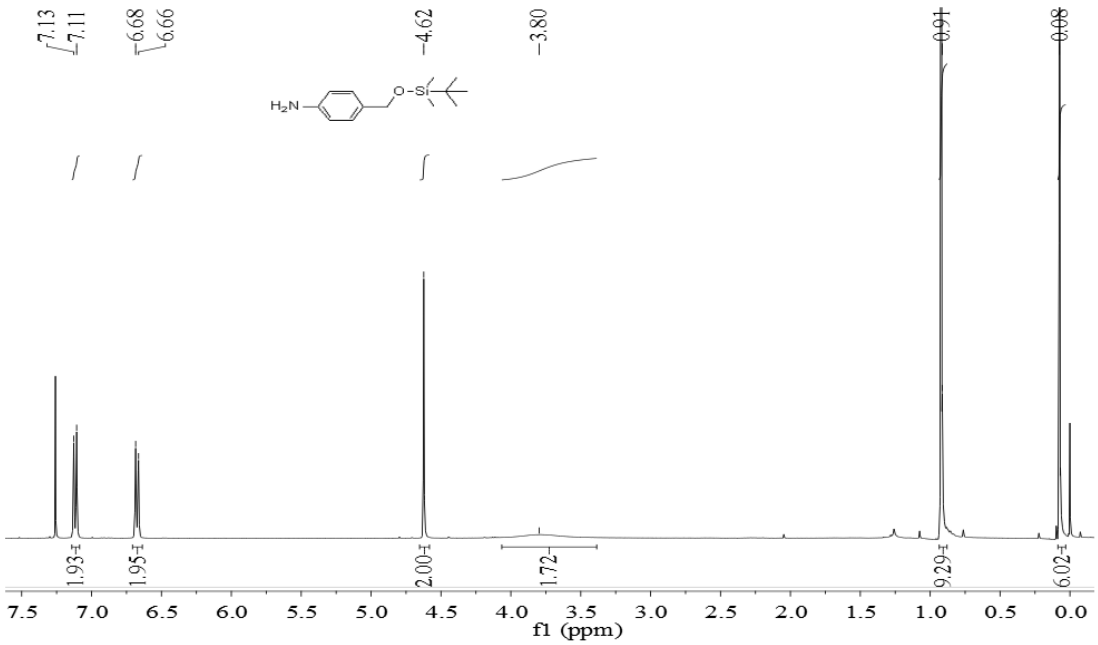

^{1}H NMR spectrum (in CDCl3) of **2**

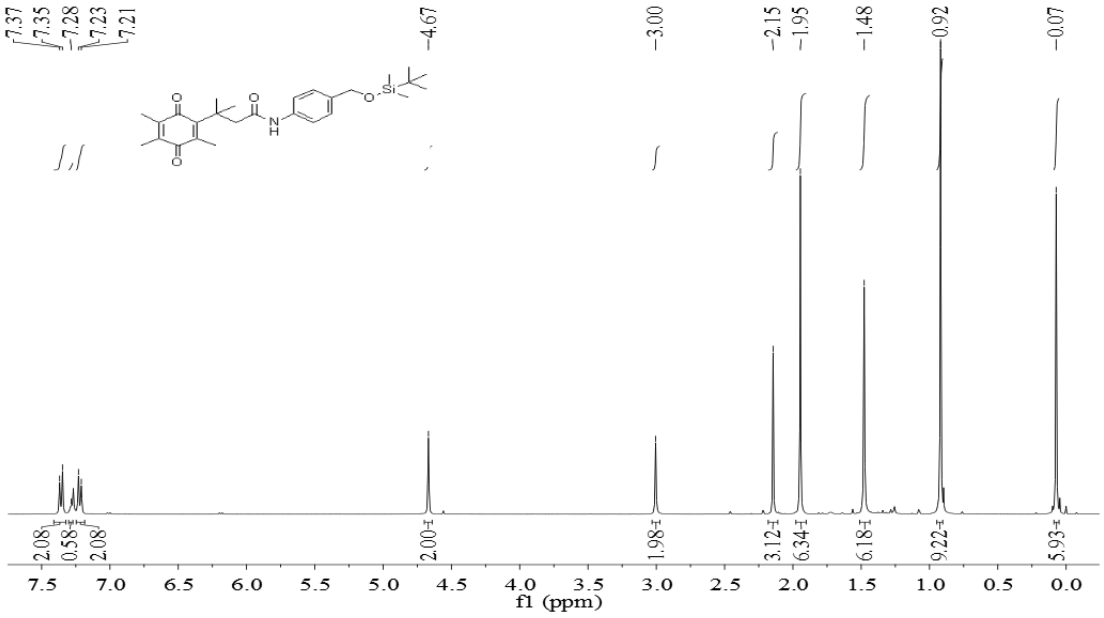

^{1}H NMR spectrum (in $CDCl_3$) of **3**

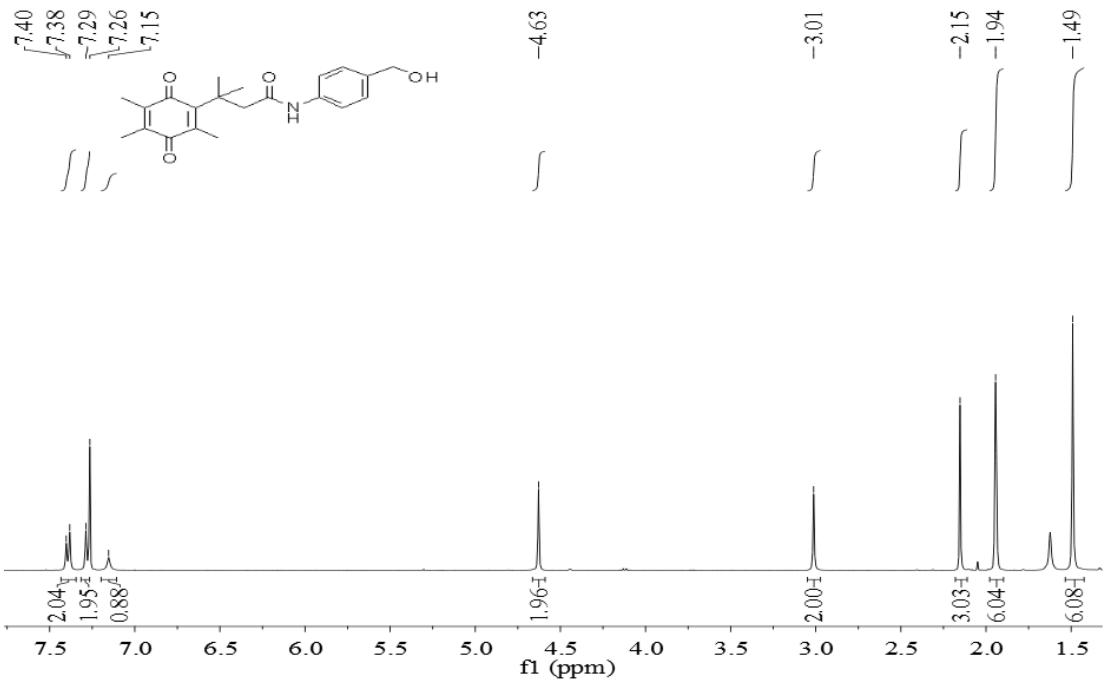

^{1}H NMR spectrum (in $CDCl_3$) of **4**

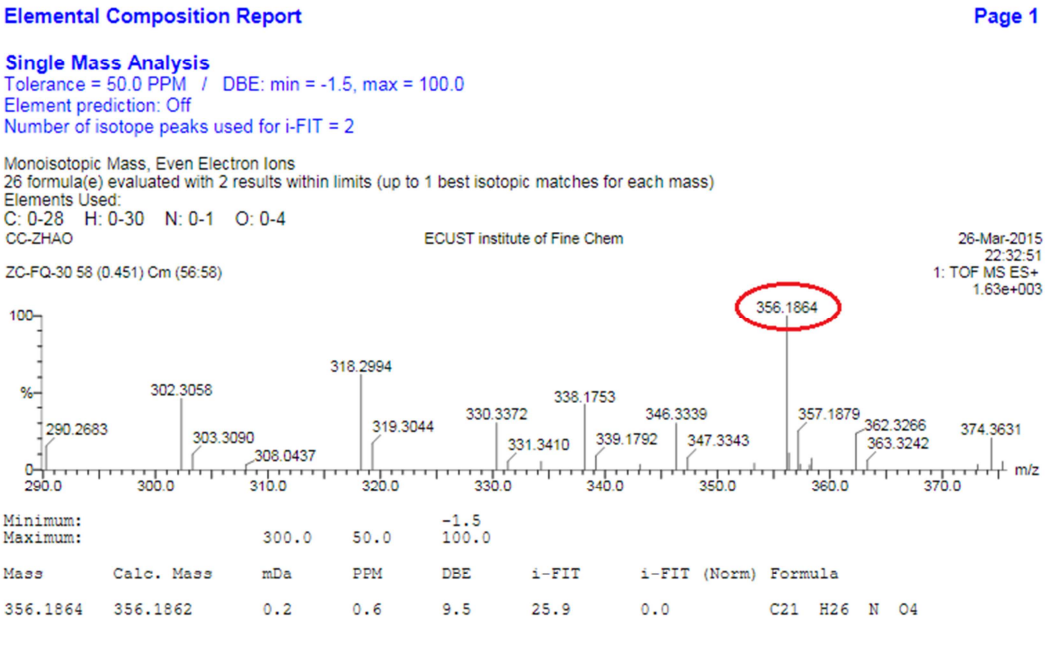

HRMS spectrum of **4**.

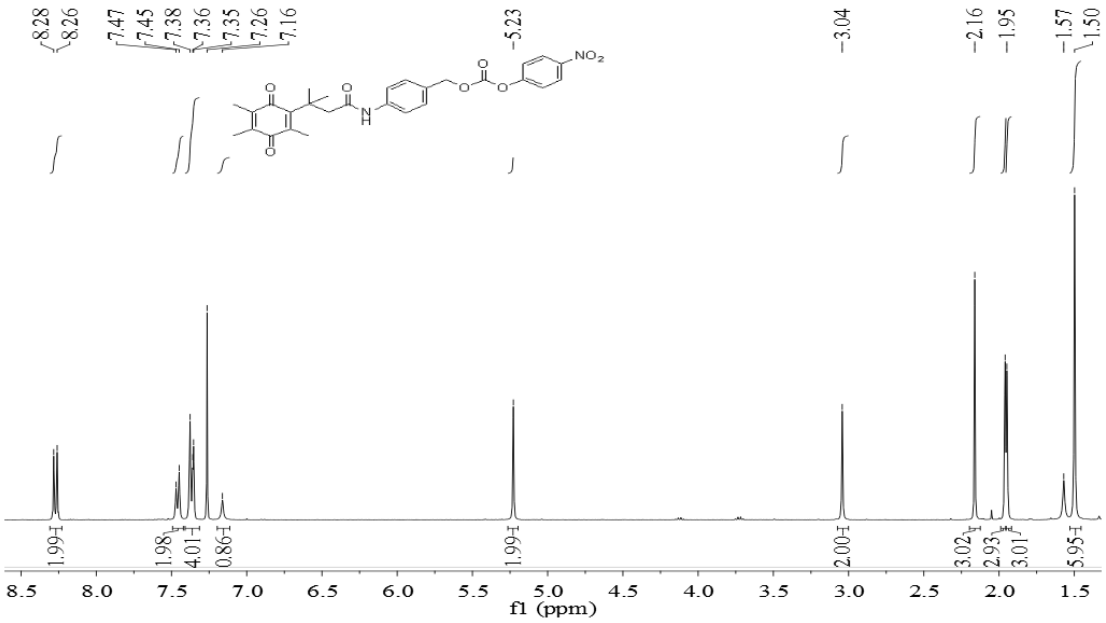

^{1}H NMR spectrum (in $CDCl_3$) of **5**

Elemental Composition Report **Page 1**

Single Mass Analysis
Tolerance = 50.0 PPM / DBE: min = -1.5, max = 100.0
Element prediction: Off
Number of isotope peaks used for i-FIT = 2

Monoisotopic Mass, Even Electron Ions
46 formula(e) evaluated with 1 results within limits (up to 1 best isotopic matches for each mass)
Elements Used:
C: 0-28 H: 0-30 N: 0-2 O: 0-8 Na: 0-1

CC-ZHAO ECUST institute of Fine Chem 26-Mar-2015 22:26:57

ZC-FQ-31 127 (0.872) Cm (122:129) 1: TOF MS ES+ 5.32e+003

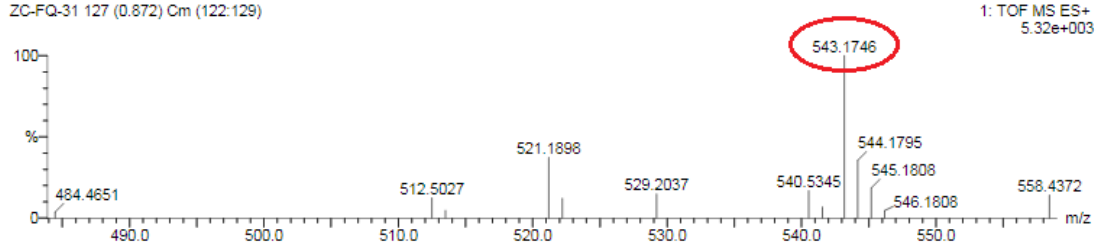

Minimum:				-1.5			
Maximum:		300.0	50.0	100.0			
Mass	Calc. Mass	mDa	PPM	DBE	i-FIT	i-FIT (Norm)	Formula
543.1746	543.1743	0.3	0.6	15.5	10.3	0.0	C28 H28 N2 O8 Na

HRMS spectrum of **5**.

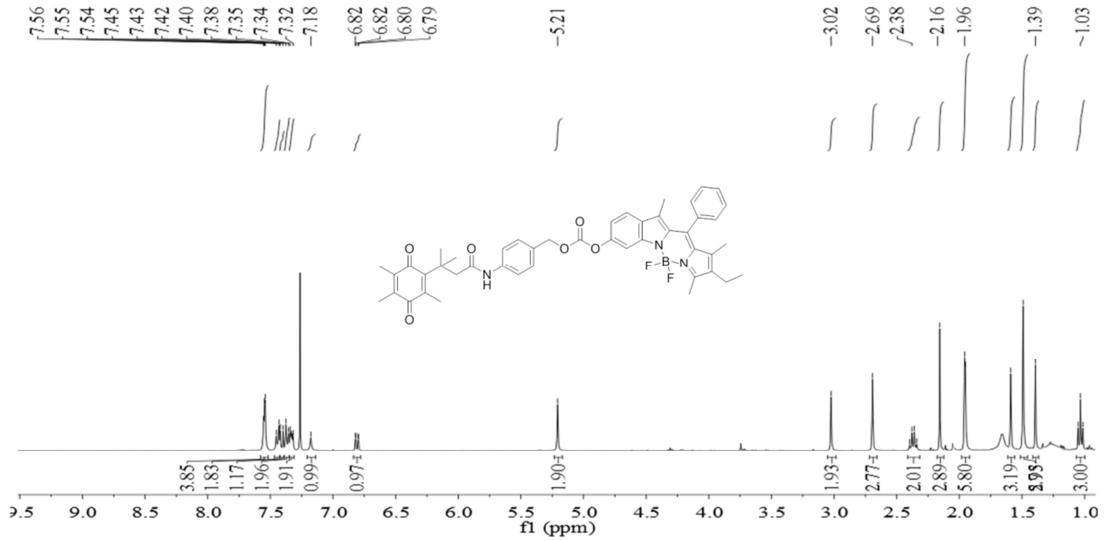

^{1}H NMR spectrum (in $CDCl_3$) of **BOD-NQO1**.

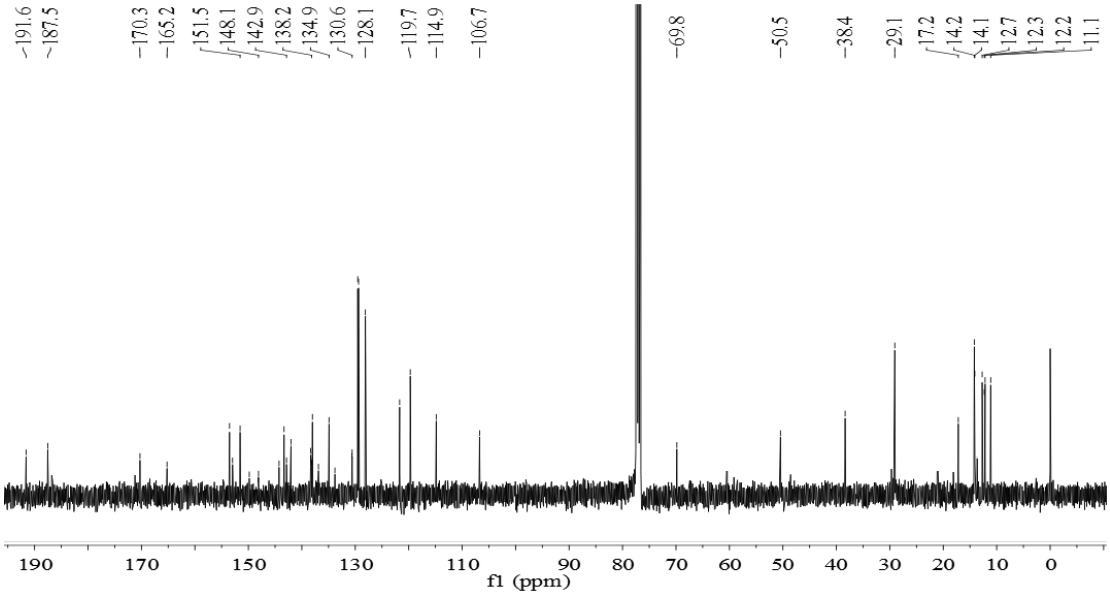

^{13}C NMR spectrum (in $CDCl_3$) of **BOD-NQO1**.

Elemental Composition Report **Page 1**

Single Mass Analysis
Tolerance = 50.0 PPM / DBE: min = -1.5, max = 100.0
Element prediction: Off
Number of isotope peaks used for i-FIT = 2

Monoisotopic Mass, Even Electron Ions
61 formula(e) evaluated with 1 results within limits (up to 1 closest results for each mass)
Elements Used:
C: 0-46 H: 0-50 B: 0-1 N: 3-3 O: 0-6 F: 0-2 Na: 0-1

CC-ZHAO ECUST institute of Fine Chem 26-Oct-2015 19:17:23

ZC-FQ-001 60 (1.921) Cm (59:61) 1: TOF MS ES+ 9.18e+002

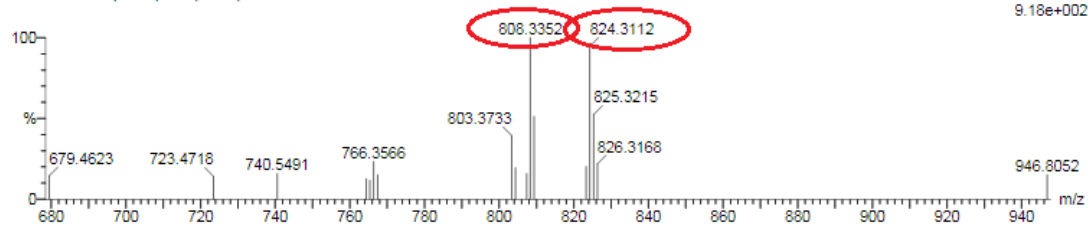

Minimum:				-1.5			
Maximum:		300.0	50.0	100.0			
Mass	Calc. Mass	mDa	PPM	DBE	i-FIT	i-FIT (Norm)	Formula
808.3352	808.3345	0.7	0.9	24.5	20.7	0.0	C46 H46 B N3 O6 F2 Na

HRMS spectrum of **BOD-NQO1**.

Highlights

1. A new NQO1-responsive small molecule was designed.

2. Polymeric micelle based nanoprobe was established for the cancer-specific NQO1.

3. Ratiometric fluorescence changes of the nanoprobe could be triggered by NQO1.

4. Differentiation between NQO1-positive and NQO1-negative cancer cells was obtained.